Electronic supplementary information to

Facile Synthesis and Efficient Electrochemiluminescence of a Readily Accessible Pyridopyrimidine

Ruizhong Zhang,[a,b] Feng Tong,[a] Liuqing Yang,[b] Jonathan Ralph Adsetts,[b] TianhaoYan,[c] Ruiyao Wang,[c] Zhifeng Ding[b]* and Hong-Bo Wang[a, b]*

[a] *Key Laboratory of Optoelectronic Chemical Materials and Devices of Ministry of Education, School of Chemical and Environmental Engineering, Jianghan University, Wuhan, Hubei 430056, China*

[b] *Department of Chemistry, The University of Western Ontario, 1151 Richmond Street, London, ON N6A 5B7, Canada*

[c] *Department of Chemistry, Xi'an Jiaotong-Liverpool University, 111 Ren'ai Road, Suzhou, Jiangsu 215123, China*

1. Additional Photoluminescence, Electrochemiluminescence, and UV-Visible Absorption Results of IPPC Compound

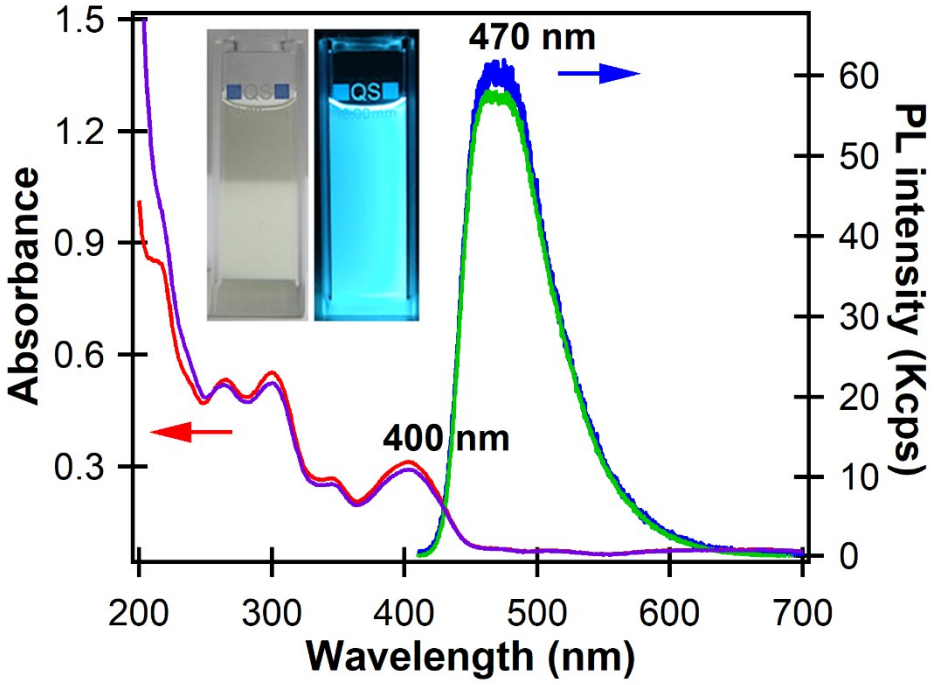

Figure S1. The UV-Visible absorption of 0.1 mM IPPC MeCN solution with (red) and without (purple) TBAP electrolyte, and PL emission spectra (excited at 400 nm) of 0.1 mM IPPC MeCN solution with (blue) and without (green) TBAP electrolyte. The insets display the photographs of the as-synthesized IPPC in MeCN solution under illumination of daylight (left) and UV (365 nm, right).

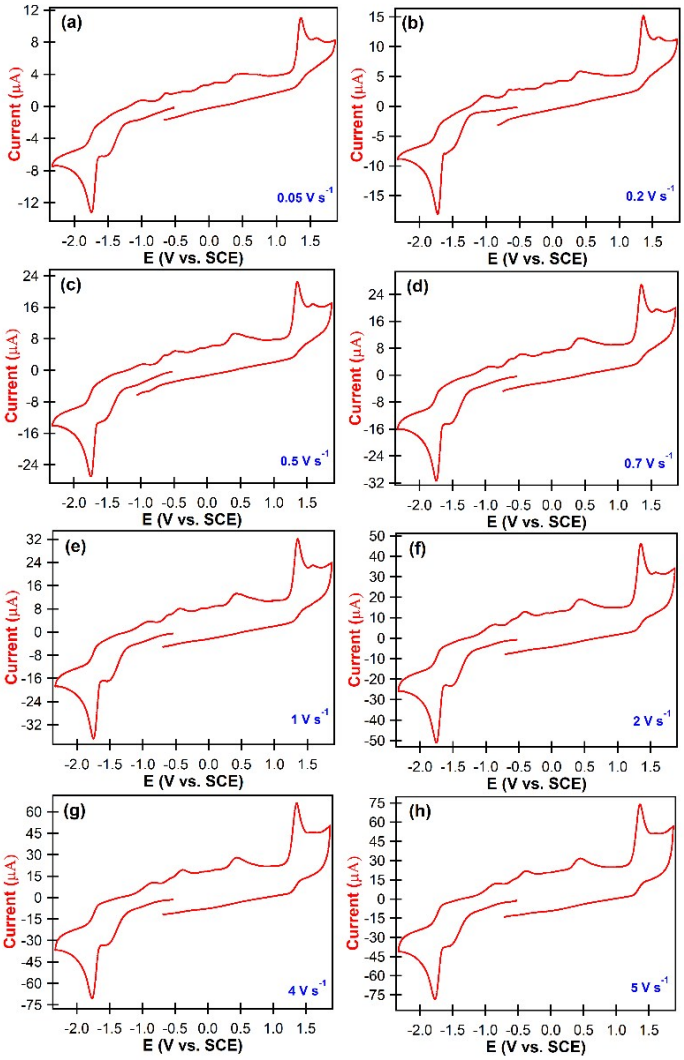

Figure S2. Cyclic voltammograms for 1.3 mM IPPC MeCN solution with 0.1 M TBAP as the supporting electrolyte at diffferent scan rate: (a) 0.05 Vs^{-1}, (b) 0.2 Vs^{-1}, (c) 0.5 Vs^{-1}, (d) 0.7 Vs^{-1}, (e) 1 Vs^{-1}, (f) 2 Vs^{-1}, (g) 4 Vs^{-1} and (h) 5 Vs^{-1}.

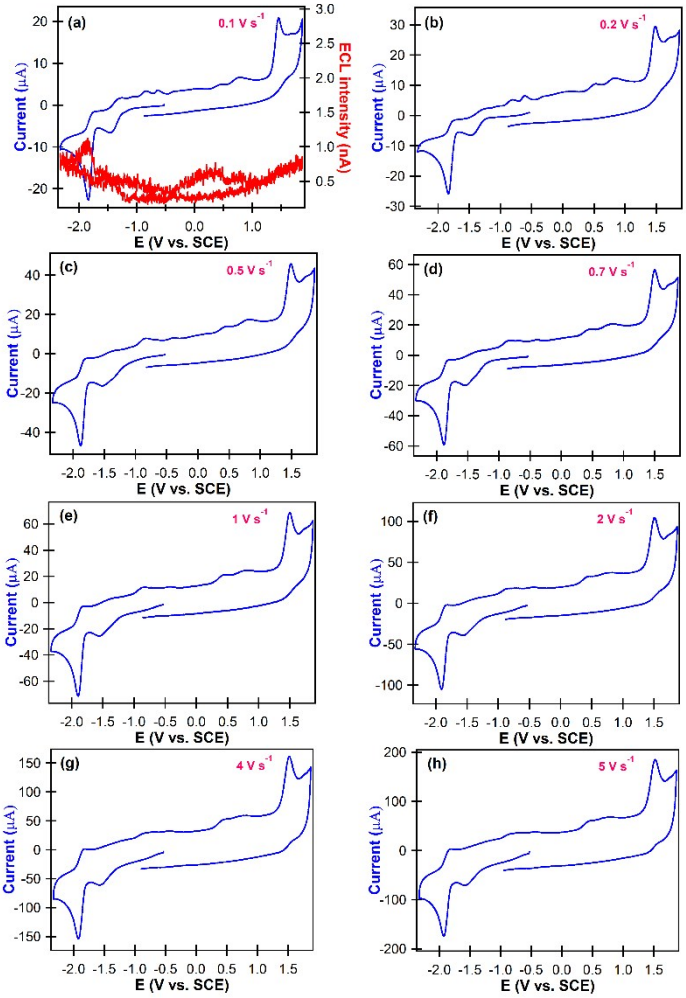

Figure S3. Cyclic voltammograms for 1.3 mM IPPC MeCN solution with 0.1 M TBAP as the supporting electrolyte at difffernet scan rate: (a) 0.1 Vs^{-1}, (b) 0.2 Vs^{-1}, (c) 0.5 Vs^{-1}, (d) 0.7 Vs^{-1}, (e) 1 Vs^{-1}, (f) 2 Vs^{-1}, (g) 4 Vs^{-1} and (h) 5 Vs^{-1} using glassy carbon electrode as the working electrode. The red curve in (a) shows the corresponding ECL-voltage curve collected with a photolultiplier (PMT, Hamanatsu R928) for the same 1.3 mM IPPC MeCN solution with 0.1 M TBAP as the supporting electrolyte.

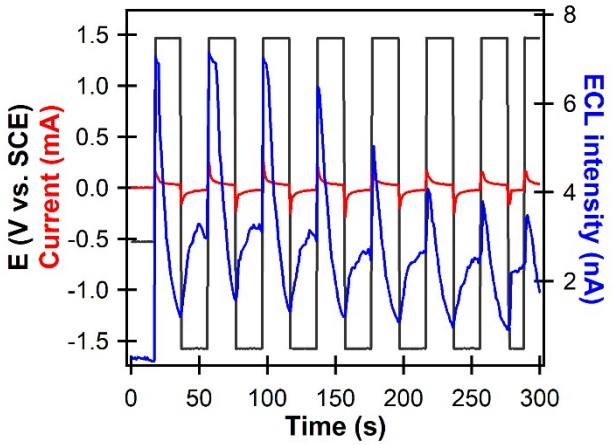

Figure S4. Curves of ECL intensity versus time and electrochemical current versus time of 1.3 mM IPPC MeCN solution with 0.1 M TBAP as the supporting electrolyte along with the applied potential profiles, recorded during the process of pulsing the working electrode between the first reduction (-1.58 V) and the first oxidation peaks (1.47 V) at a pulse width of 0.1 s.

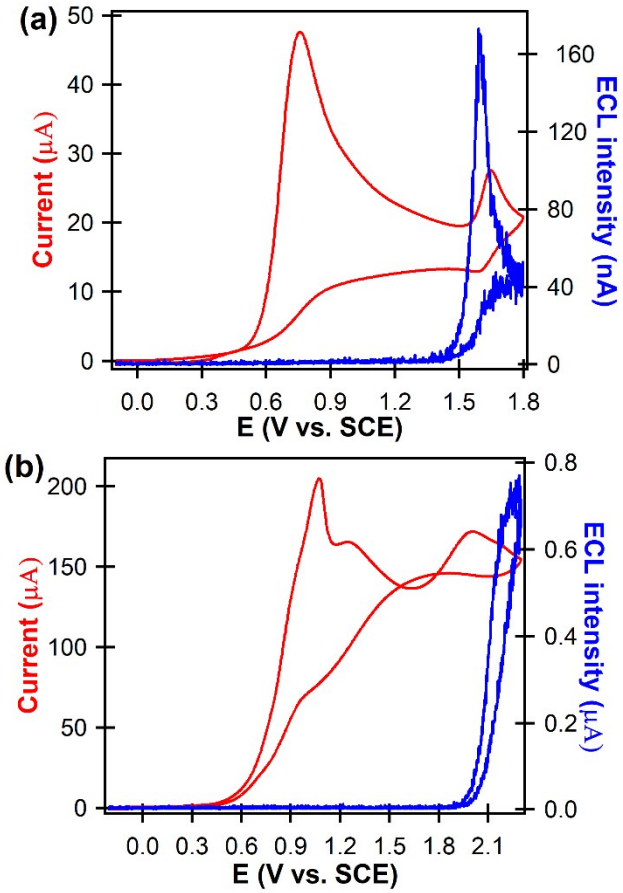

Figure S5. Cyclic voltammograms along with their corresponding ECL-voltage curves for 1.3 mM IPPC MeCN solution in the presence of (a) 5 mM TPrA and (b) 25 mM TPrA with 0.1 M TBAP as the supporting electrolyte. The scan rate was at 0.1 V s^{-1}. The ECL intensity in the ECL-voltage curve was detected as the photocurrent by a photomultiplier tube (PMT, Hamamatsu R928).

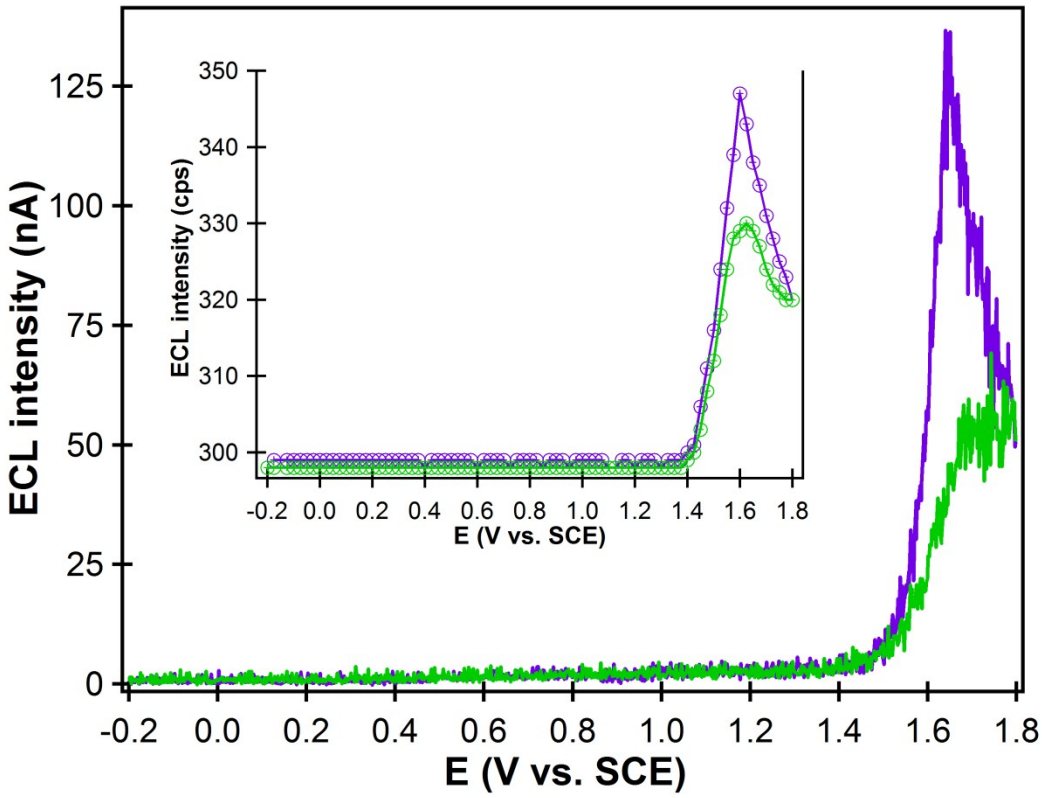

Figure S6. ECL-voltage curve obtained with a photomultiplier (PMT, Hamamatsu R928) for a 1.3 mM MeCN solution of IPPC in the presence of 5 mM TPrA and 0.1 M TBAP at a scan rate of 0.1 V s^{-1} during a potential scan cycle between -0.2 V and 1.8 V. The inset illustrates the peak intensity of spooling ECL spectra versus the applied potential (derived from Figure 2) collected with an Andor DV420-BV CCD camera (cooled at -55℃) at a time interval of 1 s or potential interval of 25 mV. Color codes: purple (forward scan, -0.2 to 1.8 V) and green (backward scan, 1.8 to -0.2 V).

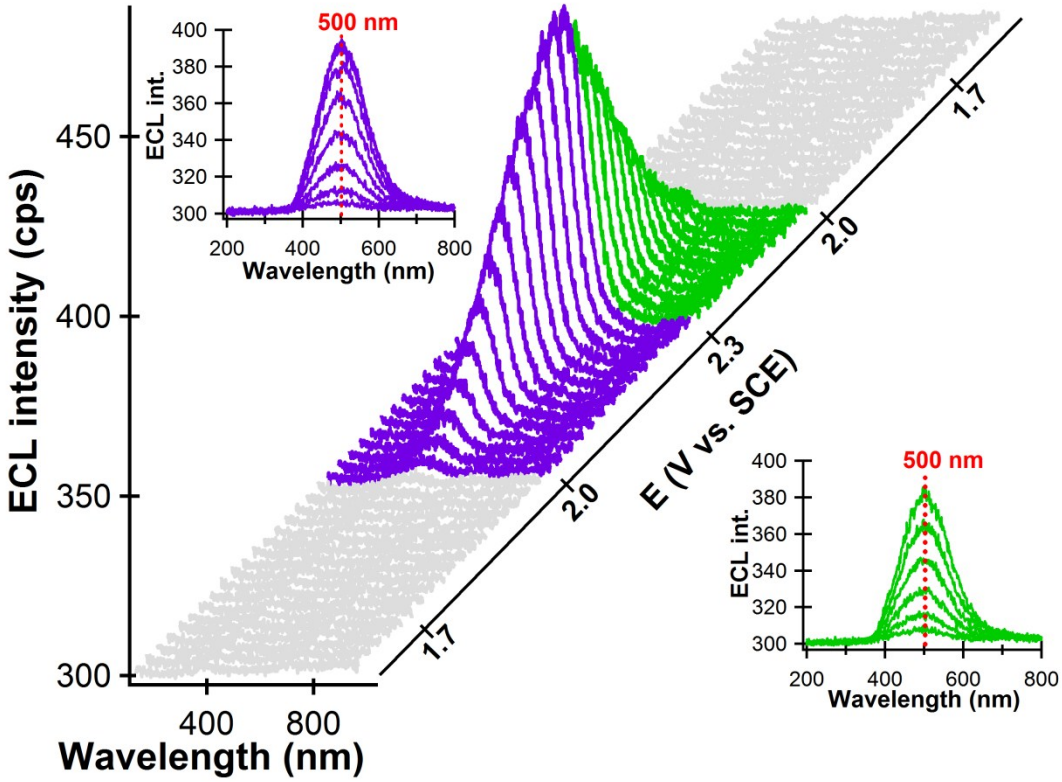

Figure S7. Spooling ECL spectra of 1.3 mM IPPC with 25 mM TPrA in MeCN containing 0.1 M TBAP during a potential scan cycle between -0.2 and 2.3 V at a scan rate of 0.025 Vs^{-1}. An Andor DV420-BV CCD camera (colled at -55℃) was used to collect the spectra at a time interval of 1 s or potential interval of 25 mV. The insets show the stacked spooling spectra for ECL evolution (purple) and devolution (green) in a better visualization. Colour codes: purple for the forward scan and green for backward scan.

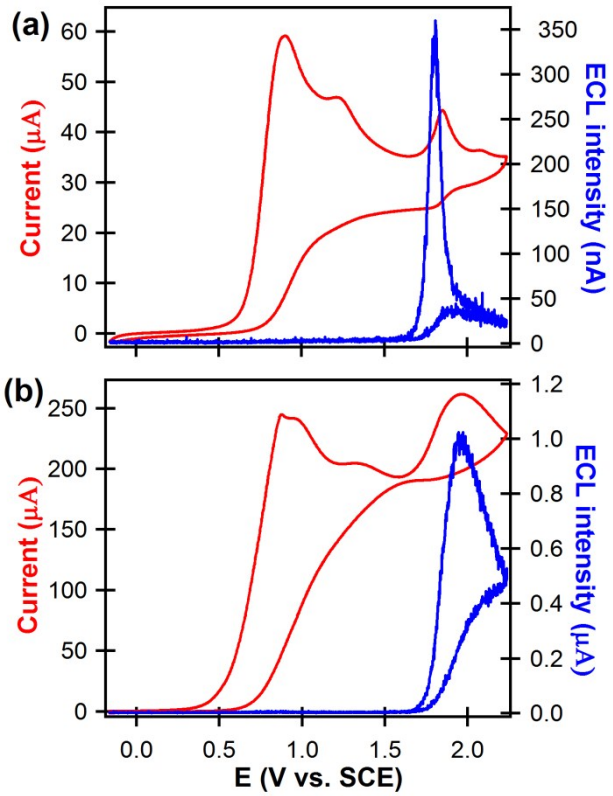

Figure S8. Cyclic voltammograms along with their corresponding ECL-voltage curves for 1.3 mM IPPC MeCN solution in the presence of (a) 5 mM DBAE and (b) 25 mM DBAE with 0.1 M TBAP as the supporting electrolyte. The scan rate was at 0.1 V s^{-1}. The ECL intensity in the ECL-voltage curve was detected as the photocurrent by a photomultiplier tube (PMT, Hamamatsu R928).

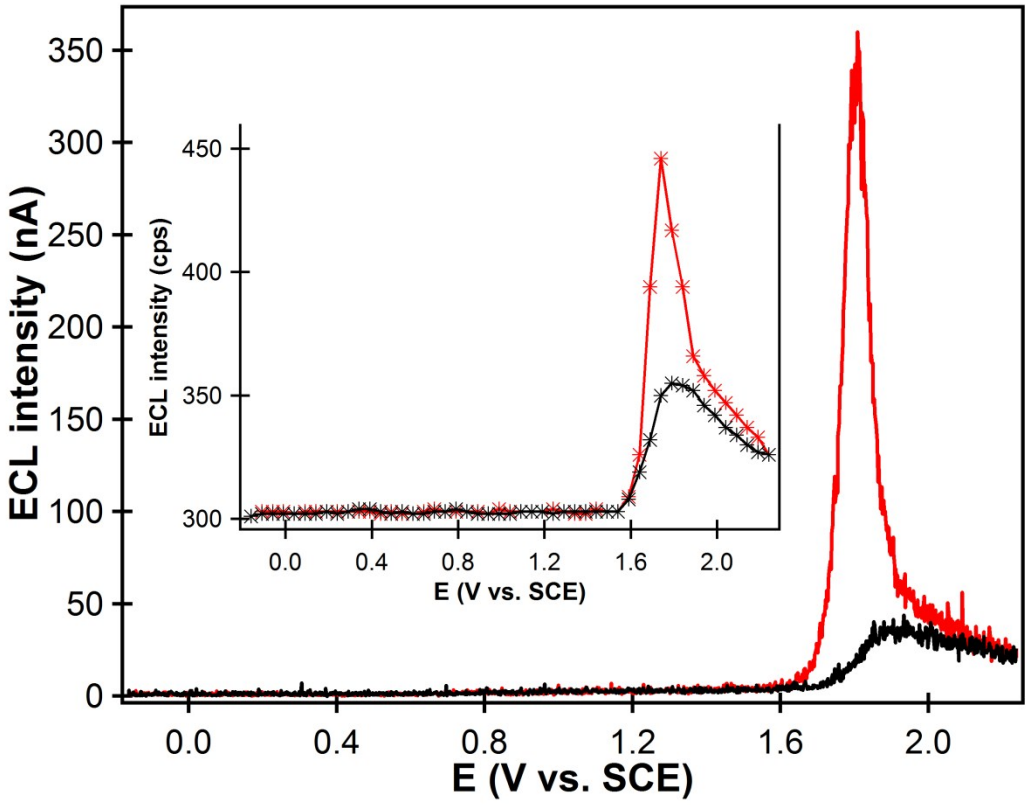

Figure S9. ECL-voltage curve obtained with a photomultiplier (PMT, Hamamatsu R928) for a 1.3 mM MeCN solution of IPPC in the presence of 5 mM DBAE and 0.1 M TBAP at a scan rate of 0.025 V s^{-1} during a potential scan cycle between -0.16 V and 2.24 V. The inset illustrates the peak intensity of spooling ECL spectra versus the applied potential (derived from Figure 3) collected with an Andor DV420-BV CCD camera (cooled at -55℃) at a time interval of 2 s or potential interval of 50 mV.. Color codes: red (forward scan, -0.16 to 2.24 V) and black (backward scan, 2.24 to -0.16 V).

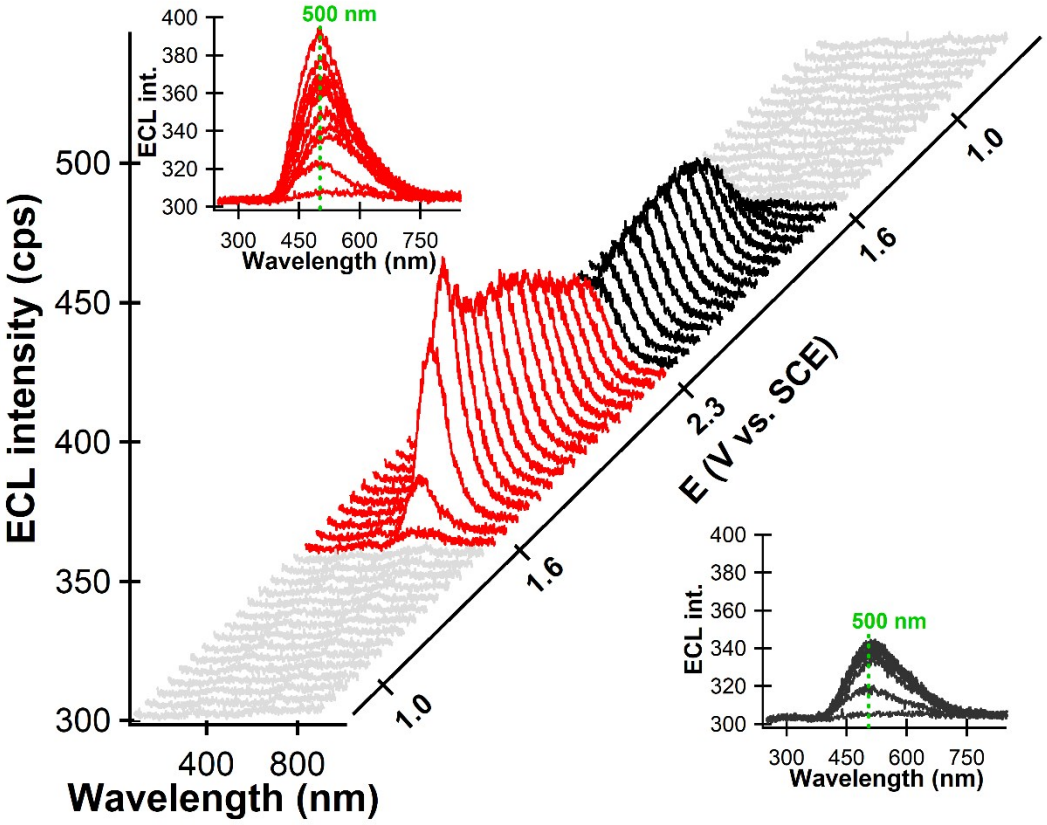

Figure S10. Spooling ECL spectra of 1.3 mM IPPC with 25 mM DBAE in MeCN containing 0.1 M TBAP during a potential scan cycle between -0.16 and 2.34 V at a scan rate of 0.05 Vs^{-1}. An Andor DV420-BV CCD camera (colled at -55℃) was used to collect the spectra at a time interval of 1 s or potential interval of 50 mV. The insets show the stacked spooling spectra for ECL evolution (red) and devolution (black) in a better visualization.

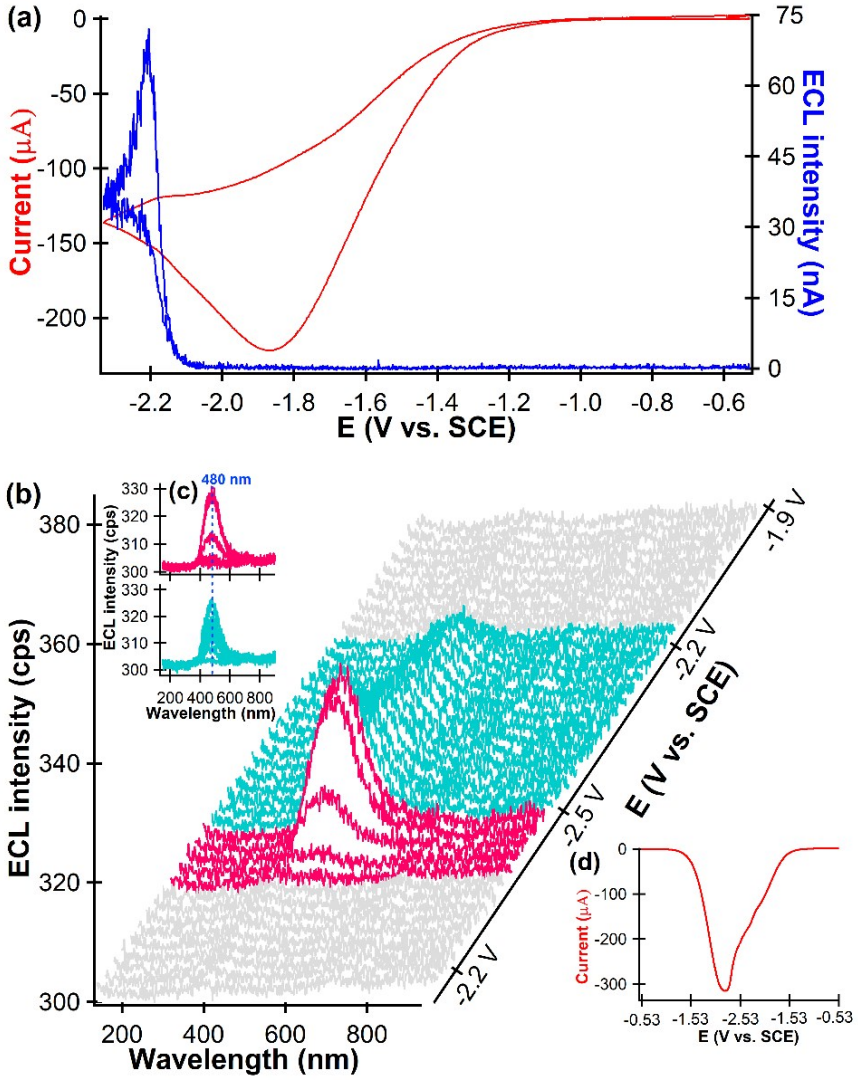

Figure S11. (a) Cyclic voltammogram along with the corresponding ECL-voltage curve for 1.3 mM IPPC MeCN solution in the presence of 15 mM BPO with 0.1 M TBAP as the supporting electrolyte. The scan rate was at 0.1 V s^{-1}. The ECL intensity in the ECL-voltage curve was detected as the photocurrent by a photomultiplier tube (PMT, Hamamatsu R928). (b) Spooling ECL spectra, (c) the stacked spooling spectra and (d) the corresponding current-voltage curve of 1.3 mM IPPC with 15 mM BPO in MeCN containing 0.1 M TBAP during a potential scan cycle between -0.53 V and -2.53 V at a scan rate of 0.25 V s^{-1}. An Andor DV420-BV CCD camera (cooled at -55℃) was used to collect the spectra at a time interval of 0.1 s or potential interval of 25 mV. Colour codes: rose red for the forward scan and greenish-blue for backward scan.

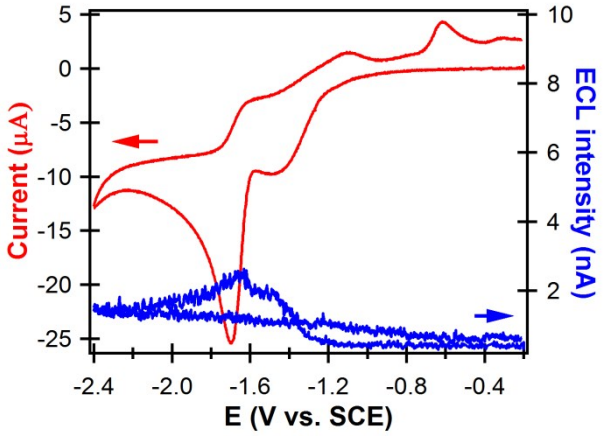

Figure S12. Cyclic voltammogram along with the corresponding ECL-voltage curve for 1.3 mM IPPC MeCN solution in the presence of 5mM $(TBA)_2S_2O_8$ with 0.1 M TBAP as the supporting electrolyte. The scan rate was at 0.1 V s^{-1}. The ECL intensity in the ECL-voltage curve was detected as the photocurrent by a photomultiplier tube (PMT, Hamamatsu R928).

Table S1. Comparison of the ECL efficiency of the present IPPC and reported organic/metal complex compounds

	Compound	Coreactant	Relative ECL efficiency ($[Ru(bpy)_3]^{2+}$ [a] or DPA [d] as the standard)	References
Metal Complexes	$Ru(bpy)_3^{2+}$		100%	
	$[Ru(BTB)Ru][PF_6]$	–	40%	1
	Ru(4-TPZ)	–	7.4%	2
	Ru(4-TBN)Me	–	11.6%	2
	Ru(4-TBN)	–	5.7%	2
	RuTPh	–	7.2%	2
	Ru(BTB)Ru	–	9.0%	2
	Ru(4TBN)Ru	–	15.3%	2
	$[Ru(bpy)_3CONH]_2$(DMBP)	–	400%	3
	$[Ru(bpy)_3CONH]_2$(DMN)	–	50%	3
	[Ir][Ru][Ir]	Tri-*n*-propylamine	2.67%	4
	$Ir(ppy)_3$	Tri-*n*-propylamine	33%	5
	$(btp)_2Ir(acac)$	Tri-*n*-propylamine	28%	6
	F(Ir)pic	Tri-*n*-propylamine	3%	6
	$[(ppy)_2Ir(bpy)]^+$	Tri-*n*-propylamine	200%	7
	$(pq)_2Ir$(**L**)	Tri-*n*-propylamine or Tetrabutylammonium persulfate	40%~1760%	8
	$[(dFphtl)_2Ir(dmabpy)]PF_6$	–	34%~550%	9
	$(phtl)_2Ir(bpy)^+$ (**1-4**)	Benzoyl peroxide	0.2%~22.4%	10
	$Ir(ppy)_2$(L) (**15**)	Tri-*n*-propylamine	20%	11
	Pt(II) complex (**Ptm**)	Tetrabutylammonium persulfate	50% and 1400%	12
	Pt1 and Pt2	Tri-*n*-propylamine Tetrabutylammonium persulfate	17% and 0.58% 0.28% and 17%	13
	$Pt\text{-}PEG_2$	Tri-*n*-propylamine	120%[b]	14
	Pt(DPP)(acac)	Tri-*n*-propylamine	87%	15
	Pt(BPP)(acac)	Tri-*n*-propylamine	91%	15
	Pt(II) salophen (**1-7**)	Tri-*n*-propylamine	0.1%~49.5%	16
	$Os(phen)_2(dppene)(PF_6)_2$	Tri-*n*-propylamine	95%	17
	$CsPbBr_3$ QDs	Tri-*n*-propylamine	500%	18
BODIPY and Derivatives	BODIPY derivative (**PM567**)	–	18%	19
	BODIPY derivative (**B[8]amide**)	Benzoyl peroxide	12%	20
	BODIPY derivative (**1-20**)	Tri-*n*-propylamine or Benzoyl peroxide	0.1%~21%	21, 22
	BOPEG(**1-3**)	Benzoyl peroxide	0.2%~20%	23
	BODIPY derivative	Tri-*n*-propylamine	58%~97%	24
	Boron difluoride formazanate dye	Tri-*n*-propylamine	15%~114%	25
	Boron difluoride formazante (**1a-1c**)	Tri-*n*-propylamine	11%~450%	26
Luminol and Composites	Luminol	–	–	27-29
	Luminol-Au NPs	–	–	30-38
	Luminol-Ag-rGO	–	–	39, 40
	Luminol-Pt@Au	–	–	41, 42
	Luminol-PtPd	–	–	43
	Luminol-Ti nanotubes	–	–	44, 45
Other Organic	9,10-Diphenylanthracene	–	28%	46
	Phenylethynylcoumarins (**1-10**)	–	0.0001~0.60[c]	47
	Triarylamine-spirobifluorenes(**D2A2**)	–	0.26%	48

Compounds	Thienyl-containing silole (**3a-4d**)	–	0.135%~24.9%	49
	Polyaromatic hydrocarbons	–	0.1%~90% [d]	50, 51
	9-Naphthylanthracene derivatives	–	0.45% [d]	52
	Deoxycytidine analogues (**1-4**)	Benzoyl peroxide	0.2%~1.87% [d]	53
	Dithienylbenzothiadiazole (**1b**)	–	81~122% [c]	54
	Flurene and Spirobifluorene (**1-2**)	–	170~300% [d]	55
	Spirofluorene dye (**1, 4 and 5**)	Tri-*n*-propylamine	5%~454%	56
	Flurene or Spirobifluorene bridge linked triphenylamines (**1-6**)	–	170%~420% [d]	57
	Thienyltriazoles (**1-4**)	Benzoyl peroxide	0.01%~0.5% [d]	58
	Thiophene-Triazole-Thiophene(**TTT**)	Tetrabutylammonium persulfate	3%	59
	IPPC	2-(Dibutylamino)ethanol	29%	**This work**

[a] The absolute ECL efficiency of $Ru(bpy)_3^{2+}$ is 0.05, and the ECL efficiencies listed in **Table S1** are relative to $Ru(bpy)_3^{2+}$ in organic systems except for the special labeled; [b] The ECL conducted in aqueous solution. [c] Relative intensity to that of $Ru(bpy)_3^{2+}$. [d]The ECL efficiency obtained using DPA as a standard, the absolute ECL efficiency of DPA is 0.014.

In comparison with the ECL efficiency listed in Table S1, it can be observed that the ECL efficiency of the present IPPC is comparable to some noble metal-based complexes but is superior to most of the reported metal-free organic compounds. Some phenylethynlcoumarines were reported with a high ECL intensity, but the relative ECL efficiency was not determined.[47] In addition, the coumarines might be expensive. Another exception is for some polyatomic hydrocarbons reported by the Bard group with an ECL efficiency up to 90% relative to DPA.[51] However, they might expensive and difficulty to make.

Although the ECL efficiency details of common used luminol have not reported, the ECL intensities for pure luminol reported in literatures are weak, therefore the combination of luminol with nanomaterials (Au NPs, Ag NPs, Ti nanotubes, etc.) or oxidase (cholesterol oxidase, glucose oxidase, etc.) are most used systems for improving the ECL performance of luminol. In these cases, an additional step for preparing luminol-nanomaterial composites or pre-modifying nanomaterials or oxidases on the electrodes is usually needed, which is less efficient than direct using bright luminophores.

Considering the much lower cost of IPPC than the noble metal-based complexes, along with the simpler, faster, greener and higher yielded synthesis of IPPC than the most reported organic compounds, the as-prepared IPPC shows great promise as an efficient luminophore for ECL application.

2. Experimental Section

Reagents and Apparatus

2-(Dibutylamino)ethanol (DBAE, 99%), tri-*n*-propylamine (TPrA, ≥ 98%), benzoyl peroxide (BPO, 97%), anhydrous acetonitrile (MeCN, 99.8%, in a Sure/Seal™ bottle that was immediately transferred into an N_2-filled glove box), tris(2,2'-bipyridyl)-ruthenium(II)hexafluorophosphate [$Ru(bpy)_3(PF_6)_2$, 98%] and ferrocene (Fc, 98%) were all purchased from Sigma-Aldrich (Mississauga, ON). The supporting electrolyte, tetra-*n*-butylammonium perchlorate (TBAP, electrochemical grade) was obtained from Alfa Aesar (Ward Hill, MA). All chemical reagents were used as received and stored at room temperature with the exception of DBAE, TPrA and BPO were stored at 4℃. ^1H (400 MHz) and ^{13}C (100 MHz) NMR spectra were recorded using Ascend™ 400 MHz spectrometer (Bruker). ^1H and ^{13}C NMR spectra were referenced relative to tetramethyl-silane (TMS) using the residual non-deuterated NMR solvent signal. X-Ray diffraction data were collected on Bruker APEX-II CCD diffractometer using monochromatic Mo-Kα radiation (λ= 0.71073 Å).

Synthesis of 4-imino-4*H*-pyrido[1,2-*a*]pyrimidine-3-carbonitrile (IPPC)

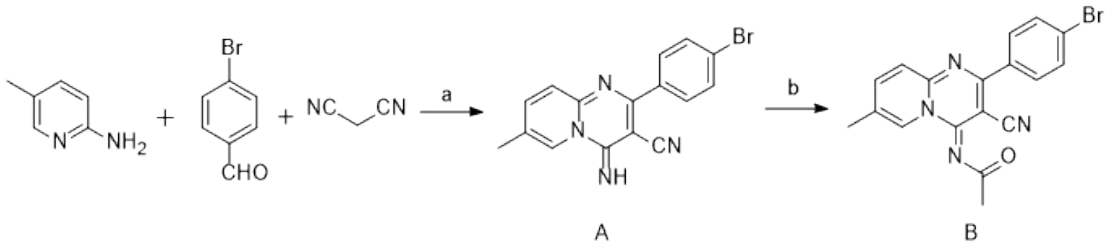

Scheme S1 (a) *L*-proline, water, 80℃, 15 min, microwave; (b) Ac_2O, 2-Me THF, reflux, 48 h.

Synthesis of Compound A: A mixture of 4-bromobenzaldehyde (1.0 g, 5.4 mmol), 2-amino-5-methylpyridine (700 mg, 6.5 mmol), malononitrile (430 mg, 6.5 mmol), and *L*-proline (125 mg, 1.08 mmol) in water of 35 mL microwave vessel (80℃, 100 W, 150 PSI, 15 min). After the reaction solution was cooled down to room temperature and extracted with dichloromethane, the organic phase was dried with anhydrous $MgSO_4$, and concentrated under reduced pressure. The residue was purified to afford bright yellow solid with 1192 mg. ^1H NMR (400 MHz, $CDCl_3$) δ 9.27 (s, 1H),

7.87 (d, J = 8.4 Hz, 2H), 7.76 (d, J = 8.9 Hz, 1H), 7.65 (d, J = 8.4 Hz, 2H), 7.57 (d, J = 9.0 Hz, 1H), 2.48 (s, 3H); ^{13}C NMR (100 MHz, $CDCl_3$) δ 161.7, 153.8, 149.9, 142.4, 135.4, 131.9, 130.2, 127.3, 126.8, 126.1, 125.8, 117.3, 85.7, 18.3; HRMS (m/z) calculated for $C_{16}H_{11}BrN_4$ 338.0167, found [M+H$^+$] 339.0175.

Synthesis of Compound B: A mixture of compound A (460 mg, 1.35 mmol) and acetic anhydride (1.9 mL, 20 mmol) were dissolved in 15 mL 2-methyltetrahydrofuran. The reaction was heated up to 110℃ stirred for 48 h. When the reaction solution was cooled down, solvent was removed under reduced pressure. The residue was purified by flash chromatography on silica gel (dichloromethane/ethyl acetate =3/1) to afford the yellow solid with 415 mg. ^{1}H NMR(400 MHz, $CDCl_3$) δ 9.08 (s, 1H), 7.87 (t, J = 7.5 Hz, 3H), 7.72 (d, J = 8.9 Hz, 1H), 7.65 (d, J = 8.5 Hz, 2H), 2.52 (s, 3H), 2.42 (s, 3H); ^{13}C NMR (100 MHz, $CDCl_3$) δ 180.5, 164.7, 149.6, 145.0, 142.9, 134.9, 131.9, 130.7, 128.8, 126.5, 116.0, 85.3, 77.0, 76.7, 27.3, 18.6; HRMS (m/z) calculated for $C_{18}H_{13}BrN_4O$ 380.0273, found 380.0278.

Photoluminescence and UV-visible Instrumentation

UV-visible spectra were recorded over a range 200-900 nm using a Varian Cary 50 spectrophotometer (Varian Inc., North Carolina). Photoluminescence (PL) experiments were conducted by using a Fluorolog instrument (QM-7/2005, Photon Technology International, London, ON) with an excitation slit width of 0.25 and an emission slit width of 0.1. All solutions for UV-visible and photoluminescence experiments were prepared in MeCN and analyzed in quartz cuvette with a path length of 1 cm.

Photoluminescence (PL) Quantum Yield Calculations

The PL quantum yield (Φ) of the studied IPPC compound was calculated by comparing the integrated photoluminescence intensities (excited at 400 nm) and the absorbance values (at 400 nm) of the IPPC with the reference quinine sulfate.[60]

Five concentrations of IPPC MeCN (refractive index (η) is 1.34) solutions were prepared, all of which had absorbance less than 0.1 at 400 nm. Quinine sulfate (literature Φ=54%) was dissolved in 0.1 M H_2SO_4 (η=1.33). The quantum yield was calculated using the following equation:

$$\Phi_x = 54\% \frac{I_x}{I_{st}} \frac{A_{st}}{A_x} \left(\frac{\eta_x}{\eta_{st}} \right)^2 \qquad \text{(S1)}$$

in which the Φ is the photoluminescence yield, I is the measured integrated PL emission intensity, A is the absorbance and η is the refractive index of the solvent. The subscript *st* refers to standard and *x* for the experimental sample.

Electrochemical Preparations

The electrochemistry and ECL of 4-imino-4*H*-pyrido[1,2-*a*]pyrimidine-3-carbonitrile (IPPC) were carried out using a 2 mm diameter Pt disc inlaid in a glass sheath as the working electrode, two coiled Pt wires as counter electrode and the quasi-reference electrode, respectively. After each experiment, the electrochemical potential window was calibrated using ferrocence as the internal standard. The redox potential of the ferrocence/ferrocenium (Fc/Fc^+) couple was taken as 0.4 V vs. SCE.[10, 25, 61] Prior to each experiment, the Pt working electrode was polished on a felt polishing pad (Buehler Ltd., Lake Bluff, IL) using 1.0 and 0.05 μm alumina suspensions (Buehler Ltd.) in ultrapure water (18.2 MΩ cm, Milli-Q, Millipore) consecutively for 5 min each to obtain a mirror-like surface. The working electrode was then washed with copious amounts of ultrapure water. The working electrode was further electrochemically polished in 0.1 M H_2SO_4 for 200 cycles between the approximate potentials between -1.0 V and 1.0 V at 0.5 Vs^{-1} to obtain a clean and more reproducible Pt surface. The working electrode was then washed repeatedly with ultrapure water and dried with a stream of Ar gas (ultrahigh purity, ＞99.9%, Praxair Canada Inc., London, ON) over the Pt disc area and left to dry for 12 h at room temperature. The counter and reference electrodes were rinsed with acetone, followed by deionized water. They were then sonicated in isopropanol (10 min) and ultrapure water (5 min) before thorough rinsing with ultrapure water. These electrodes were dried at 120℃ and left to cool to room temperature before use.

Prior to experiments, the electrochemical cell was rinsed with isopropanol, acetone and ultrapure water, followed by immersion in a base bath of 5% KOH in isopropanol for 4 h. The cell was rinsed with copious ultrapure water and immersed in an acid bath of 1% HCl for 4 h. After finishing in acid bath, the electrochemical cell was rinsed thoroughly with ultrapure water, dried at 120℃ for 12 h and then cooled to room temperature. This cleaning method was used since it provides a more

thorough cleaning of our electrochemical cell. This electrochemical cell was specifically designed to have a Pyrex window at the bottom to allow the detection of generated light (ECL) from the working electrode vicinity. In annihilation ECL studies, a solution containing approximately 1.3 mM of 4-imino-4*H*-pyrido[1,2-*a*]pyrimidine-3-carbonitrile (IPPC), 0.1 M TBAP as the supporting electrolyte and 3.0 mL anhydrous acetonitrile (MeCN) was added to the electrochemical cell, which was assembled in a glove box and the cell was sealed using a custom-made Teflon cap with a rubber O-ring and was removed from the glove box to perform electrochemistry and ECL experiments. For coreactant studies, aliquot volumes of commercially availabe reducing corectants (TPrA or DBAE) or aliquot masses of oxidizing coreactants[$(TBA)_2S_2O_8$ or BPO] were added to each annihilation solution under Ar blanket to prevent oxygen entering the sample solution.

Electrochemical Instrumentation

All electrochemical experiments were conducted on a CHI 610A electrochemical analyzer (CH Instruments, Austin, TX). The experimental parameters for cyclic voltammograms (CVs) are listed here: 0.000 V initial potential in experimental scale, positive or negative initial scan polarity, 0.1 V s^{-1} scan rate, 4 sweep segments, 0.001 V sample interval, 2 s quite time, $(1\text{-}5)\times10^{-5}$ A V^{-1} sensitivity.

ECL Instrumentation

For ECL measurements, the ECL-voltage curve and CV were collected simultaneously using a custom-made LabVIEW program (ECL-PMT610a.vi, National Instruments, Austin, TX). The ECL intensity was detected as a photocurrent by a photomultiplier tube (PMT, R928, Hamamatsu, Japan) held at -750 V with a high voltage power supply and transformed to a voltage signal using a picoammeter/voltage source (Keithley 6487, Cleveland, OH). The sensitivity on the picoammeter was set manually in order to avoid photosaturation. The ECL/CV signals were sent simultaneously through a DAQ board (DAQ 6052E, National Instruments, Austin, TX) in the computer workstation.

Pulsing ECL experiments were conducted by putting the photoelectrochemical cell inside the PMT compartment while still connected to the picoammeter/voltage setup. A bipotentiostat (model AFCBPI, Pine Instrument Co., Grove City, PA) and an EG&G PAR 175 Universal Programmer

(Princeton Applied Research, Trenton, NJ) were used to control the potential pulsing profile between the first oxidation and reduction peak potentials of the IPPC analyte. The pulsing potential was set to 100 mV past the peak potentials of the first oxidation wave and the first reduction wave. This assembly allowed pulsing experiments to occur without a delay, at a relative fast time pace (10 Hz). Another homemade LabVIEW programm (ECL_PAR.vi, National Instruments) was used to record the the current, potential and ECL in the pulsing experiments.

Accumulated ECL spectra were obtained by placing the electrochemical cell onto a spectrometer (Cornerstone 260, Newport, Canada) attached to a CCD camera (Model DV420-BV, Andor Technology, Belfast, UK). The camera was cooled to -55℃ prior to use, and controlled by a computer for operation and data acquisition. The intensities versus wavelengths (ECL spectra) were recorded by Andor Technology program. Similar to the CV experiments, the samples were scanned between their redox potentials. Spooling ECL spectra was recorded with the same spectrometer and camera with these of accumulated ECL spectra (the spectrometer was centered at 413 nm using a 121 *l*/nm grating) by gradually scanning between the initial potential and the first potential that resulted in emission. Collection parameters for the spooling spectra varied depending on the experimental conditions: exposure time and number in kinetic series were optimized to produce the clearest ECL spectra. During Spooling experiments, the CHI 610A electrochemical analyzer and the Andor Technology program was run to collect the CV and spectra simultaneously, and the lights in the labrotary were switched off to reduce the background interference. Blackout curtains were also positioned at the entryways to the lab and surrounding the electrochemical cell setup to prevent light interference. Wavelength calibration was accomplished using a mercury-argon source (Ocean Optics, HG-1). The data acquisition was carried out by means of an Andor Technology program.

ECL Efficiency Calculations

ECL quantum efficiency (Φ_x) was calculated relative to $Ru(bpy)_3(PF_6)_2$ system by taking its ECL efficiency as 100% in MeCN.[62-64] This was done by taking the sum of the integration of both the ECL intensity and current values (versus time) for the compound against the standard, as described in the following equation S2:

$$\Phi_x = 100\% \frac{\left[\frac{\int_a^b ECL \, \mathrm{dt}}{\int_a^b Current \, \mathrm{dt}}\right]_x}{\left[\frac{\int_a^b ECL \, \mathrm{dt}}{\int_a^b Current \, \mathrm{dt}}\right]_{st}} \qquad \text{(S2)}$$

where *x* and *st* represent studied sample and the standard, respectively. Equation S2 is based on the principle of generated photos per electron.

ECL experiments for each compound were tested with a minimum of five different potential windows based on their redox potentials, tuning for the strongest ECL activity.

Theoretical Calculations

For the HOMO-LUMO theoretical calculations with Gaussian 03, the molecular conjugation of IPPC was optimized under DFT/B3LYP/6-31G(d) level by using ONIOM model.

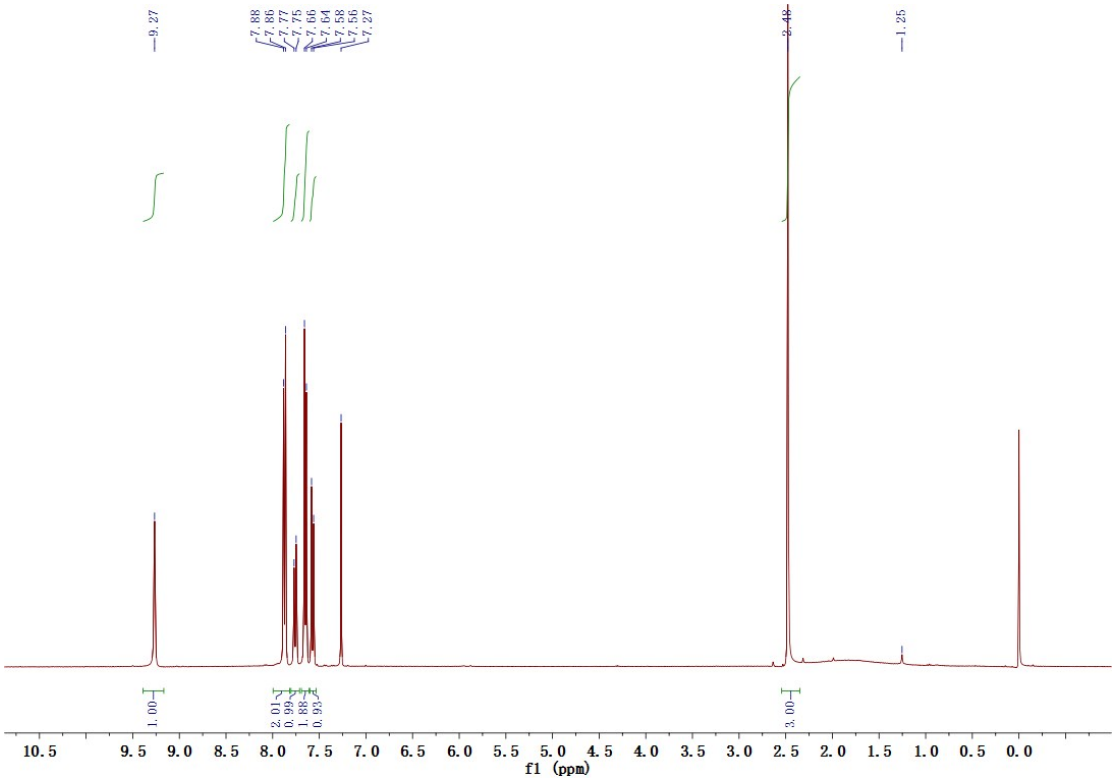

Figure S13. ^{1}H NMR spectrum of Compound A

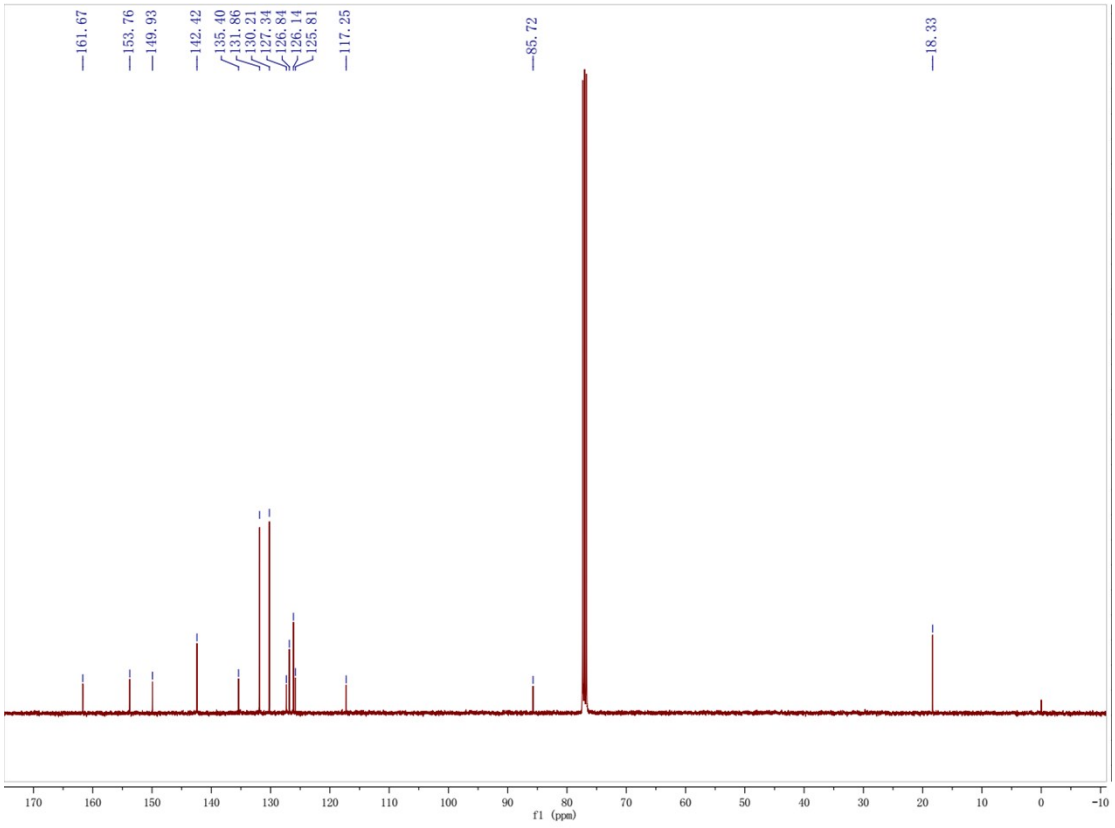

Figure S14. ^{13}C NMR spectrum of Compound A

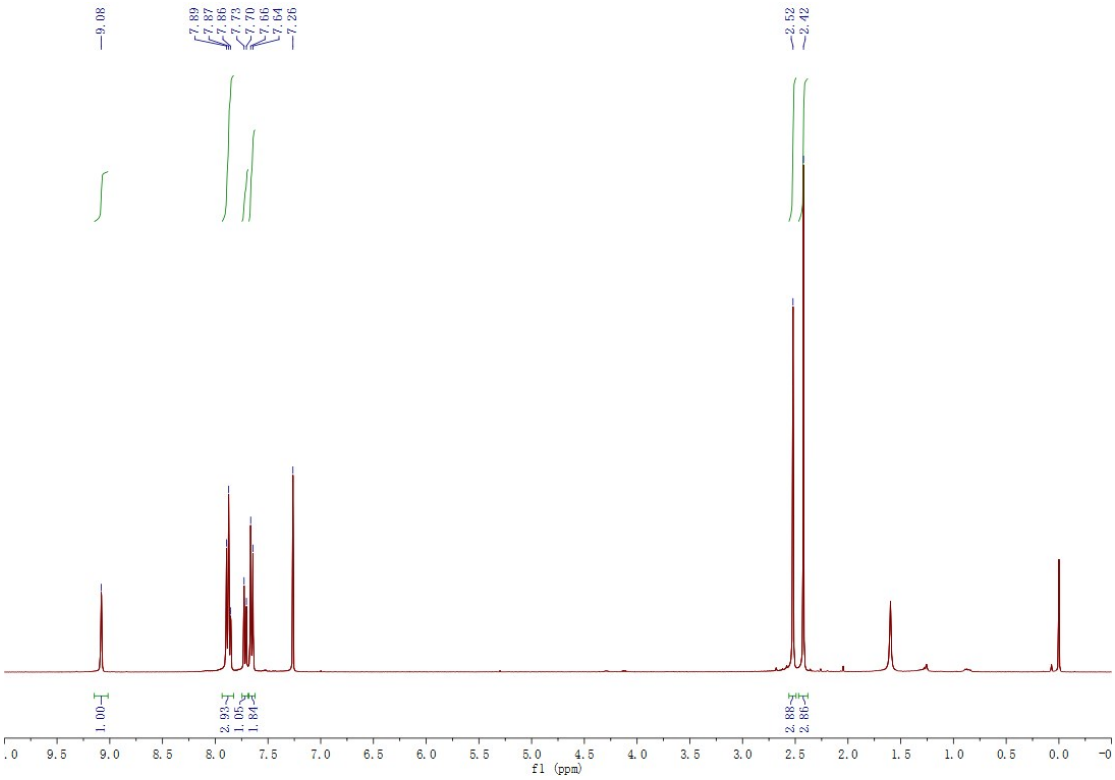

Figure S15. ^{1}H NMR spectrum of Compound B

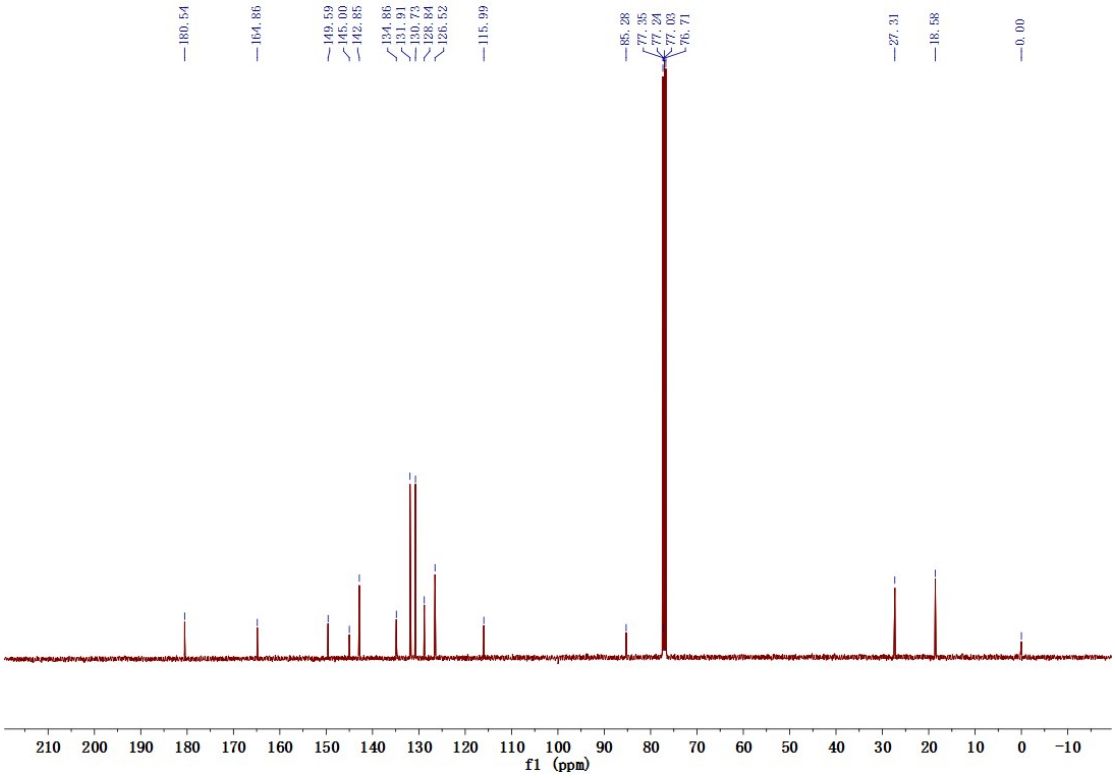

Figure S16. ^{13}C NMR spectrum of Compound B

References

1. S. Stagni, A. Palazzi, S. Zacchini, B. Ballarin, C. Bruno, M. Marcaccio, F. Paolucci, M. Monari, M. Carano and A. J. Bard, *Inorg. Chem.*, 2006, **45**, 695-709.
2. S. Zanarini, A. J. Bard, M. Marcaccio, A. Palazzi, F. Paolucci and S. Stagni, *J. Phys. Chem. B*, 2006, **110**, 22551-22556.
3. M. N. Li, J. H. Liu, C. Z. Zhao and L. C. Sun, *J. Organomet. Chem.*, 2006, **691**, 4189-4195.
4. K. N. Swanick, M. Sandroni, Z. Ding and E. Zysman-Colman, *Chem. Eur. J.*, 2015, **21**, 7435-7440.
5. D. Bruce and M. M. Richter, *Anal. Chem.*, 2002, **74**, 1340-1342.
6. B. D. Muegge and M. M. Richter, *Anal. Chem.*, 2004, **76**, 73-77.
7. J. I. Kim, I. S. Shin, H. Kim and J. K. Lee, *J. Am. Chem. Soc.*, 2005, **127**, 1614-1615.
8. I. S. Shin, J. I. Kim, T. H. Kwon, J. I. Hong, J. K. Lee and H. Kim, *J. Phys. Chem. C*, 2007, **111**, 2280-2286.
9. K. N. Swanick, S. Ladouceur, E. Zysman-Colman and Z. Ding, *Angew. Chem. Int. Ed.*, 2012, **51**, 11079-11082.
10. K. N. Swanick, S. Ladouceur, E. Zysman-Colman and Z. Ding, *Chem. Commun.*, 2012, **48**, 3179-3181.
11. B. D. Stringer, L. M. Quan, P. J. Barnard, D. J. D. Wilson and C. F. Hogan, *Organometallics*, 2014, **33**, 4860-4872.
12. S. He, X. Wang, G. Xiang, K. Lac, S. Wang and Z. Ding, *Electrochim. Acta*, 2018, DOI: https://doi.org/10.1016/j.electacta.2018.03.056.
13. G. Xiang, X. Wang, M. S. M. Li, K. Lac, S. Wang and Z. Ding, *ChemElectroChem*, 2017, DOI: 10.1002/celc.201700059, n/a-n/a.
14. S. Carrara, A. Aliprandi, C. F. Hogan and L. De Cola, *J. Am. Chem. Soc.*, 2017, **139**, 14605-14610.
15. C. X. Li, S. Q. Wang, Y. M. Huang, B. Zheng, Z. Q. Tian, Y. H. Wen and F. Li, *Dalton Trans.*, 2013, **42**, 4059-4067.
16. E. F. Reid, V. C. Cook, D. J. D. Wilson and C. F. Hogan, *Chem-Eur J*, 2013, **19**, 15907-15917.
17. D. Bruce, M. M. Richter and K. J. Brewer, *Anal. Chem.*, 2002, **74**, 3157-3159.
18. J. J. Xue, Z. Y. Zhang, F. F. Zheng, Q. Xu, J. C. Xu, G. Z. Zou, L. L. Li and J. J. Zhu, *Anal. Chem.*, 2017, **89**, 8212-8216.
19. R. Y. Lai and A. J. Bard, *J. Phys. Chem. B*, 2003, **107**, 5036-5042.
20. M. M. Sartin, F. Camerel, R. Ziessel and A. J. Bard, *J. Phys. Chem. C*, 2008, **112**, 10833-10841.
21. A. B. Nepomnyashchii, S. Cho, P. J. Rossky and A. J. Bard, *J. Am. Chem. Soc.*, 2010, **132**, 17550-17559.
22. A. B. Nepomnyashchii and A. J. Bard, *Acc. Chem. Res.*, 2012, **45**, 1844-1853.
23. A. B. Nepomnyashchii, A. J. Pistner, A. J. Bard and J. Rosenthal, *J. Phys. Chem. C*, 2013, **117**, 5599-5609.
24. M. Hesari, J. Lu, S. Wang and Z. Ding, *Chem. Commun.*, 2015, **51**, 1081-1084.
25. M. Hesari, S. M. Barbon, V. N. Staroverov, Z. Ding and J. B. Gilroy, *Chem. Commun.*, 2015, **51**, 3766-3769.
26. M. Hesari, S. M. Barbon, R. B. Mendes, V. N. Staroverov, Z. F. Ding and J. B. Gilroy, *J. Phys. Chem. C*, 2018, **122**, 1258-1266.
27. X. Y. Liu, W. J. Qi, W. Y. Gao, Z. Y. Liu, W. Zhang, Y. Gao and G. B. Xu, *Chem. Commun.*, 2014, **50**, 14662-14665.
28. G. Z. Ma, J. Y. Zhou, C. X. Tian, D. C. Jiang, D. J. Fang and H. Y. Chen, *Anal. Chem.*, 2013, **85**, 3912-3917.
29. W. Wang, H. Cui, Z. X. Deng, Y. P. Dong and J. Z. Guo, *J. Electroanal. Chem.*, 2008, **612**, 277-287.
30. J. N. Shu, W. Wang and H. Cui, *Chem. Commun.*, 2015, **51**, 11366-11369.
31. X. Y. Jiang, H. J. Wang, R. Yuan and Y. Q. Chai, *Biosenson.Bioelectron.*, 2015, **63**, 33-38.
32. H. R. Zhang, M. S. Wu, J. J. Xu and H. Y. Chen, *Anal. Chem.*, 2014, **86**, 3834-3840.
33. F. Li, Y. Q. Yu, H. Cui, D. Yang and Z. P. Bian, *Analyst*, 2013, **138**, 1844-1850.
34. Y. L. Cao, R. Yuan, Y. Q. Chai, L. Mao, H. Niu, H. J. Liu and Y. Zhuo, *Biosens. Bioelectron.*, 2012, **31**, 305-309.
35. Y. Chai, D. Y. Tian, W. Wang and H. Cui, *Chem. Commun.*, 2010, **46**, 7560-7562.
36. W. Wang, T. Xiong and H. Cui, *Langmuir*, 2008, **24**, 2826-2833.
37. Y. P. Dong, H. Cui and Y. Xu, *Langmuir*, 2007, **23**, 523-529.
38. H. Cui, W. Wang, C. F. Duan, Y. P. Dong and J. Z. Guo, *Chem. Eur. J*, 2007, **13**, 6975-6984.

39. X. Y. Jiang, Y. Q. Chai, H. J. Wang and R. Yuan, *Biosens. Bioelectron.*, 2014, **54**, 20-26.
40. C. M. Wang and H. Cui, *Luminescence*, 2007, **22**, 35-45.
41. Y. Zhou, Y. Zhuo, N. Liao, Y. Q. Chai and R. Yuan, *Chem. Commun.*, 2014, **50**, 14627-14630.
42. X. Y. Jiang, Y. Q. Chai, R. Yuan, Y. L. Cao, Y. F. Chen, H. J. Wang and X. X. Gan, *Anal. Chim. Acta*, 2013, **783**, 49-55.
43. Y. L. Cao, R. Yuan, Y. Q. Chai, H. J. Liu, Y. H. Liao and Y. Zhuo, *Talanta*, 2013, **113**, 106-112.
44. G. F. Xu, X. X. Zeng, S. Y. Lu, H. Dai, L. S. Gong, Y. Y. Lin, Q. P. Wang, Y. J. Tong and G. N. Chen, *Luminescence*, 2013, **28**, 456-460.
45. Y. Y. Lin, H. Dai, G. F. Xu, T. Yang, C. P. Yang, Y. J. Tong, Y. S. Yang and G. N. Chen, *Microchim Acta*, 2013, **180**, 563-572.
46. J. T. Maloy and A. J. Bard, *J. Am. Chem. Soc.*, 1971, **93**, 5968-5981.
47. A. Elangovan, J. H. Lin, S. W. Yang, H. Y. Hsu and T. I. Ho, *J. Org. Chem.*, 2004, **69**, 8086-8092.
48. F. Fungo, K. T. Wong, S. Y. Ku, Y. Y. Hung and A. J. Bard, *J. Phys. Chem. B*, 2005, **109**, 3984-3989.
49. C. Booker, X. Wang, S. Haroun, J. G. Zhou, M. Jennings, B. L. Pagenkopf and Z. F. Ding, *Angew. Chem. Int. Ed.*, 2008, **47**, 7731-7735.
50. W. J. Miao, *Chem. Rev.*, 2008, **108**, 2506-2553.
51. K. M. Omer, S. Y. Ku, K. T. Wong and A. J. Bard, *Angew. Chem. Int. Ed.*, 2009, **48**, 9300-9303.
52. J. Suk, Z. Y. Wu, L. Wang and A. J. Bard, *J. Am. Chem. Soc.*, 2011, **133**, 14675-14685.
53. K. N. Swanick, D. W. Dodd, J. T. Price, A. L. Brazeau, N. D. Jones, R. H. E. Hudson and Z. Ding, *Phys. Chem. Chem. Phys.*, 2011, **13**, 17405-17412.
54. M. Shen, J. Rodriguez-Lopez, J. Huang, Q. A. Liu, X. H. Zhu and A. J. Bard, *J. Am. Chem. Soc.*, 2010, **132**, 13453-13461.
55. F. Polo, F. Rizzo, M. Veiga-Gutierrez, L. De Cola and S. Quici, *J. Am. Chem. Soc.*, 2012, **134**, 15402-15409.
56. H. D. Li, J. Daniel, J. B. Verlhac, M. Blanchard-Desce and N. Sojic, *Chem-Eur J*, 2016, **22**, 12702-12714.
57. F. Rizzo, F. Polo, G. Bottaro, S. Fantacci, S. Antonello, L. Armelao, S. Quici and F. Maran, *J. Am. Chem. Soc.*, 2017, **139**, 2060-2069.
58. K. N. Swanick, J. T. Price, N. D. Jones and Z. Ding, *J. Org. Chem.*, 2012, **77**, 5646-5655.
59. M. Li, K. Chu, J. T. Price, N. Jones and Z. Ding, *ChemElectroChem*, 2016, **3**, 2170-2178.
60. J. Zhou, C. Booker, R. Li, X. Zhou, T.-K. Sham, X. Sun and Z. Ding, *J. Am. Chem. Soc.*, 2007, **129**, 744-745.
61. N. G. Connelly and W. E. Geiger, *Chem. Rev.*, 1996, **96**, 877-910.
62. W. L. Wallace and A. J. Bard, *J. Phys. Chem.*, 1979, **83**, 1350-1357.
63. P. Mccord and A. J. Bard, *J. Electroanal. Chem.*, 1991, **318**, 91-99.
64. J. E. Bartelt, S. M. Drew and R. M. Wightman, *J. Electrochem. Soc.*, 1992, **139**, 70-74.